Thermoelectric Materials

DOI: 10.1002/ange.200600865

High Thermoelectric Figure of Merit and Nanostructuring in Bulk p-type $Na_{1-x}Pb_mSb_yTe_{m+2}$**

*Pierre F. P. Poudeu, Jonathan D'Angelo, Adam D. Downey, Jarrod L. Short, Timothy P. Hogan, and Mercouri G. Kanatzidis**

Thermoelectric materials are special types of semiconductors that function as "heat pumps" and as heat-to-electricity converters. Thermoelectric power generation allows for small size, high reliability, and quiet operation. Efficient thermoelectric-based heat-to-electricity converters require higher performance materials than are currently available.[1,2] Direct conversion of heat to electricity could be achieved with solid-state devices based on thermoelectric materials. These devices could play an important role in future energy production, conversion, management, and utilization. When a temperature gradient is created across a thermoelectric

[*] Dr. P. F. P. Poudeu, Prof. M. G. Kanatzidis
Department of Chemistry
Michigan State University
East Lansing, MI 48824 (USA)
Fax: (+1) 517-353-1793
E-mail: kanatzid@cem.msu.edu

J. D'Angelo, A. D. Downey, J. L. Short, Prof. T. P. Hogan
Department of Electrical and Computer Engineering
Michigan State University
East Lansing, MI 48824 (USA)

[**] Financial support from the Office of Naval Research (MURI program) is gratefully acknowledged.

Supporting information for this article is available on the WWW under http://www.angewandte.org or from the author.

module, a voltage is generated, owing to the Seebeck effect. This voltage can be used to drive an external load.[3] Currently, there is a strong scientific and technological drive to identify new materials with enhanced thermoelectric figures of merit $ZT=(\sigma S^2/\kappa)T$ (where σ is the electrical conductivity, S the thermopower or Seebeck coefficient, κ the thermal conductivity, and T the temperature). The numerator σS^2 is called the power factor PF. Several classes of materials are currently under investigation, including complex chalcogenides,[4] doped PbTe and its solid solutions, such as $Pb_{1-x}Sn_xTe$,[5,6] superlattice thin films,[7,8] and quantum-dot superlattices.[9–11] Also of interest are skutterudites,[12,13] metal oxides,[14] and intermetallic clathrates.[15–17] The superlattice thin-film structures of Bi_2Te_3/Sb_2Te_3 grown from chemical vapor deposition,[18] and of $PbSe_{0.98}Te_{0.02}$/PbTe formed by molecular beam epitaxy (MBE)[11,19,20] have figures of merit greater than $ZT=2$ (at approximately 300 and 550 K, respectively). The MBE-grown thin films $PbSe_{0.98}Te_{0.02}$/PbTe are n-type materials and contain pyramid-shaped "nanodots" of PbSe of uniform size (approximately 20 nm), which form spontaneously inside a matrix of PbTe.[11,19,20] Because energy-conversion applications require materials in large quantities, we seek bulk analogues of these systems with similar figures of merit.

A recent contribution to these efforts was the discovery of the n-type Ag-based tellurides $AgSbTe_2$/PbTe, which can exhibit high figures of merit ($ZT\approx1.7$ at 700 K) when properly doped.[21,22] To construct a fully functioning optimal thermoelectric device, both n- and p-type materials are needed. To date, there is no p-type counterpart to $AgSbTe_2$/PbTe with similar performance. The highest figure of merit reported for p-type bulk materials ($ZT\approx1.2$ at 700 K) is exhibited by the so-called TAGS system (based on Te, Ag, Ge, and Sb: $(GeTe)_{1-x}((Ag_2Te)_{1-y}(Sb_2Te_3)_y)_x$).[23] These Ge-containing materials, though more efficient than PbTe, have found limited use, owing to their high cost and to a low-temperature phase transition. Recently, we described the p-type materials $Ag(Pb_{1-y}Sn_y)_mSbTe_{2+m}$, which show outstanding thermoelectric properties, reaching a maximum figure of merit of $ZT\approx1.45$ at 630 K.[24]

Herein, we report that the Ag-free system $Na_{1-x}Pb_mSb_yTe_{m+2}$, with appropriate combinations of m, y, and x, achieves record-high ZT values for a p-type bulk thermoelectric material. The effect of the composition on the thermoelectric properties is profound. We show that the high performance of these materials derives mainly from a low thermal conductivity. High-resolution transmission electron microscopy (HRTEM) demonstrates pervasive nanostructuring in $Na_{1-x}Pb_mSb_yTe_{m+2}$, which may be the root cause for the remarkably low thermal conductivity.[25] The $Na_{1-x}Pb_mSb_yTe_{m+2}$ system was selected for study because it should be naturally prone to create Na, Sb-rich clusters in the lattice. The distribution of Na^+ and Sb^{3+} ions in the Pb^{2+} sublattice cannot be random, as would be demanded by a solid solution, because Coulombic forces alone tend to drive the system to clustering at the nanoscale, thereby lowering the overall energy.[26] The results described herein are in agreement with long-standing theoretical predictions that nanostructuring in semiconductors would lead to enhanced thermoelectric figures of merit.[25,27] The $Na_{1-x}Pb_mSb_yTe_{m+2}$ materials could find applications in devices for power generation from a wide variety of hot sources, for example, vehicle exhausts, coal-burning installations, or electric power utilities.

$Na_{1-x}Pb_mSb_yTe_{m+2}$ ($y\leq1$) samples (see Supporting Information for synthesis details[28]) exhibit p-type conduction from 300 to 700 K. Ingots with the composition $Na_{0.95}Pb_{19}SbTe_{21}$ ($m=19$, $x=0.05$, $y=1$) exhibit an electrical conductivity of $\sigma=1422\ S\,cm^{-1}$ with a positive thermopower of $S=105\ \mu V\,K^{-1}$ at room temperature. This leads to the relatively high power factor of $PF=15.6\ \mu W\,cm^{-1}\,K^{-2}$. The temperature dependence of the electrical conductivity and the thermopower of $Na_{0.95}Pb_{19}SbTe_{21}$ are shown in Figure 1 A.

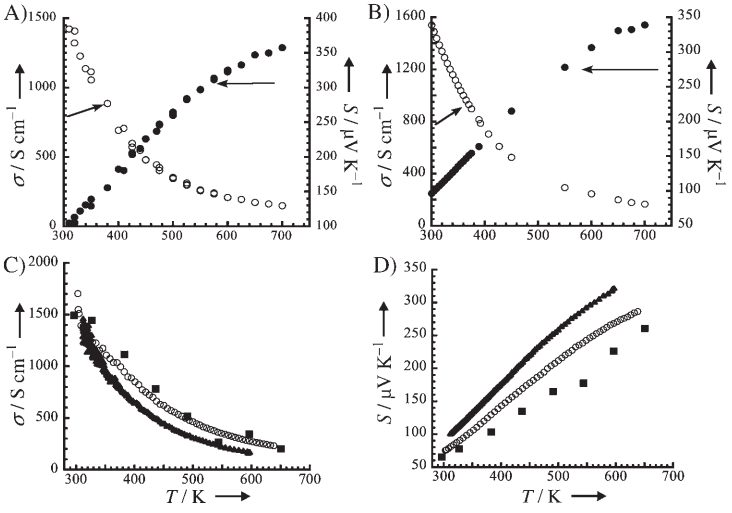

Figure 1. Temperature dependence of the electrical conductivity σ (○) and the Seebeck coefficient S (●) for A) $Na_{0.95}Pb_{19}SbTe_{21}$ and B) $Na_{0.95}Pb_{20}SbTe_{22}$. Temperature dependence of C) the electrical conductivity σ and D) the Seebeck coefficient S for $Na_{0.8}Pb_{20}Sb_yTe_{22}$ with $y=0.4$ (■), 0.6 (○), and 0.8 (▲). The conductivity and thermopower measurements were performed simultaneously on samples of typical size $7\times5\times4\ mm^3$. See Supporting Information for measurement details.[28]

The conductivity decreases with increasing temperature, which is consistent with degenerate semiconductors, and reaches $\sigma=150\ S\,cm^{-1}$ at 700 K. However, the thermopower increases rapidly to $S=357.6\ \mu V\,K^{-1}$ at 700 K, yielding a much higher power factor of $PF=19\ \mu W\,cm^{-1}\,K^{-2}$.

For samples of composition $Na_{0.95}Pb_{20}SbTe_{22}$ ($m=20$, $x=0.05$, $y=1$), an electrical conductivity of $\sigma=1541\ S\,cm^{-1}$ and a thermopower of $S=96\ \mu V\,K^{-1}$ were measured, which result in a power factor of $PF=14.2\ \mu W\,cm^{-1}\,K^{-2}$ at 300 K. As observed for $Na_{0.95}Pb_{19}SbTe_{21}$, the electrical conductivity decreases rapidly with rising temperature (Figure 1 B). At 700 K, the conductivity is $\sigma=165\ S\,cm^{-1}$ and the thermopower is $S=339\ \mu V\,K^{-1}$, yielding a power factor of $PF=19\ \mu W\,cm^{-1}\,K^{-2}$. Therefore, the electrical performance (power factor) of $Na_{1-x}Pb_mSb_yTe_{m+2}$ samples remains almost

unchanged upon small variation of m for a constant Na/Sb ratio.

To study the influence of the Na/Sb ratio on the properties of the materials, samples with compositions $Na_{0.8}Pb_{20}Sb_yTe_{22}$, ($m = 20$, $x = 0.2$, $y = 0.4$, 0.6, 0.8) were examined. As shown in Figure 1C, the electrical conductivity increases slightly with decreasing Sb content. The drop in conductivity with rising temperature is more pronounced as the Na/Sb ratio decreases. The room-temperature Seebeck coefficient of the $Na_{0.8}Pb_{20}Sb_yTe_{22}$ samples tends to increase with decreasing Na/Sb ratio (Figure 1D). As the temperature increases, a more substantial divergence is observed in the thermopower plots, which suggests higher performance at high temperatures with decreasing Na/Sb ratio. From Figure 2A, we can

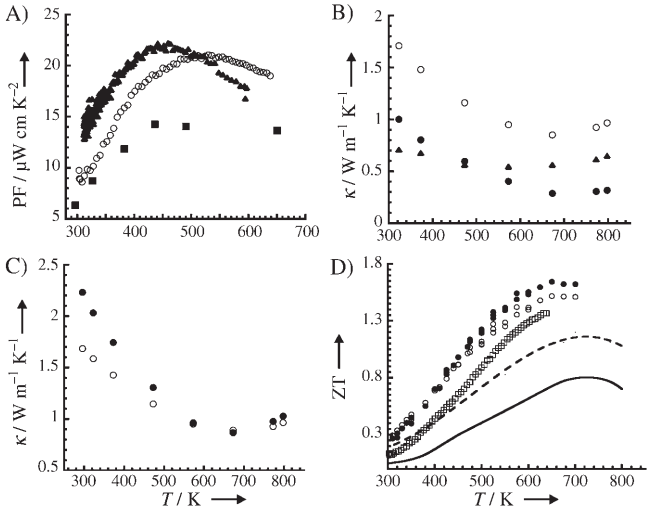

Figure 2. A) Temperature dependence of the power factor $PF = \sigma S^2$ for $Na_{0.8}Pb_{20}Sb_yTe_{22}$ with $y = 0.4$ (■), 0.6 (○), and 0.8 (▲). B) Temperature dependence of the thermal conductivity κ of $Na_{0.95}Pb_{20}SbTe_{22}$ (○), showing the lattice κ_{latt} (▲) and carrier κ_{el} (●) contributions. See text for details. C) Temperature dependence of the thermal conductivity κ of $Na_{0.95}Pb_{19}SbTe_{21}$ (○) and $Na_{0.8}Pb_{20}Sb_{0.6}Te_{22}$ (●). D) Temperature dependence of the thermoelectric figure of merit ZT for $Na_{0.95}Pb_{20}SbTe_{22}$ (●), $Na_{0.95}Pb_{19}SbTe_{21}$ (○), and $Na_{0.8}Pb_{20}Sb_{0.6}Te_{22}$ (□), compared to those of the state-of-the-art p-type materials PbTe (solid line) and TAGS (dashed line). See Supporting Information for measurement details.[28]

see that the power factor of the $Na_{0.8}Pb_{20}Sb_yTe_{22}$ materials at room temperature increases with decreasing Na/Sb ratio. The highest power factor of $PF = 22\ \mu W\,cm^{-1}\,K^{-2}$ is found for the sample with Na/Sb = 1 ($y = 0.8$) at 450 K. At 600 K, the sample with $y = 0.6$ showed a power factor of $PF = 19.5\ \mu W\,cm^{-1}\,K^{-2}$, which is the highest among the $Na_{1-x}Pb_mSb_yTe_{m+2}$ samples for this temperature.

The temperature dependence of the thermal conductivity of $Na_{0.95}Pb_{20}SbTe_{22}$, along with the lattice and carrier contributions to the thermal conductivity, are plotted in Figure 2B. At room temperature, the total thermal conductivity of the sample is $\kappa = 1.8\ W\,m^{-1}\,K^{-1}$, which is approximately 22% lower than the typical value of $\kappa = 2.3\ W\,m^{-1}\,K^{-1}$ reported for p-type PbTe.[29] The thermal conductivity decreases with increasing temperature, reaching a minimum of $\kappa = 0.85\ W\,m^{-1}\,K^{-1}$ at 675 K, and then increasing slightly from 675 to 800 K. The lattice thermal conductivity κ_{latt} was determined by subtracting the electronic contribution κ_{el} as calculated using the Wiedemann–Franz law ($\kappa_{el} = L\sigma T$, where $L \approx 2.45 \times 10^{-8}\ W\,\Omega\,K^{-2}$ is the Lorenz number) from the total thermal conductivity (that is, $\kappa_{latt} = \kappa - \kappa_{el}$). The value of $\kappa_{latt} = 0.74\ W\,m^{-1}\,K^{-1}$ at 300 K is only one third of that of PbTe ($\kappa_{latt} = 2.2\ W\,m^{-1}\,K^{-1}$).[6] Below 500 K, the thermal conductivity is mostly due to the electronic contribution, whereas above 500 K, the lattice contribution dominates. The $Na_{0.95}Pb_{19}SbTe_{21}$ and $Na_{0.80}Pb_{20}Sb_{0.6}Te_{22}$ samples also show low thermal conductivities with a temperature dependence similar to that of $Na_{0.95}Pb_{20}SbTe_{22}$ (Figure 2C). For both samples, the thermal conductivity drops very rapidly with rising temperature and reaches a minimum value of $\kappa = 0.85\ W\,m^{-1}\,K^{-1}$ near 700 K. The lattice contribution reaches a minimum of $\kappa_{latt} = 0.55\ W\,m^{-1}\,K^{-1}$, which approaches the values reported for the superlattice thin films of $PbSe_{0.98}Te_{0.02}$/PbTe ($\kappa_{latt} \approx 0.35\ W\,m^{-1}\,K^{-1}$).[11,20]

In Figure 2D, the figures of merit for the $Na_{1-x}Pb_mSb_yTe_{m+2}$ samples calculated from the above data are compared to those of the state-of-the-art p-type TAGS and PbTe-based materials. $Na_{0.95}Pb_{20}SbTe_{22}$ outperforms both systems at their individual temperatures of maximum ZT (near 700 K). At 300 K, the figure of merit of $Na_{0.95}Pb_{20}SbTe_{22}$ ($ZT \approx 0.25$) is already four times larger than that of doped p-type PbTe and 1.3 times larger than that of TAGS. More interestingly, the figure of merit of $Na_{0.95}Pb_{20}SbTe_{22}$ rises dramatically with temperature, reaches $ZT = 1$ near 475 K, and then reaches $ZT \approx 1.7$ at 650 K. The figure of merit is above $ZT = 1$ over a temperature range of approximately 300 K. This is one of the widest temperature ranges of high thermoelectric efficiency reported for a single material. Likewise, the figures of merit of $Na_{0.95}Pb_{19}SbTe_{22}$ and $Na_{0.8}Pb_{20}Sb_{0.6}Te_{22}$ reach their highest values of $ZT \approx 1.5$ and 1.4 at 650 and 640 K, respectively.

Why do the $Na_{1-x}Pb_mSb_yTe_{m+2}$ materials exhibit such good thermoelectric properties? The key characteristic is their exceptionally low thermal conductivity. The thermal conductivity of a material is typically reduced by large mass-fluctuation disorder in one atomic position of its crystal structure (random-alloy disorder, point defects, and grain boundaries). However, the large drop observed here may suggest the existence of additional mechanisms. Recently, it has been suggested that nanostructuring in bulk samples could produce strong phonon scattering.[25] While the conventional disorder condition is very likely present in our samples, the presence of nanostructuring can only be probed through a detailed examination of the structure at the atomic scale. Thus, we performed HRTEM on numerous pieces of various $Na_{1-x}Pb_mSb_yTe_{m+2}$ ingots.

HRTEM images of $Na_{0.95}Pb_{20}SbTe_{22}$ samples, for example, revealed frequent nanoscale features thought to be favorable for phonon scattering. In Figure 3A, two distinct domains with notably different atomic spacings, which have cocrystallized at the nanoscale, can be seen. The corresponding fast Fourier transforms (FFTs) of the two domains in the HRTEM image reveal a doubling of the periodicity in one direction for domain (a) with respect to the cubic spacing of domain (b),

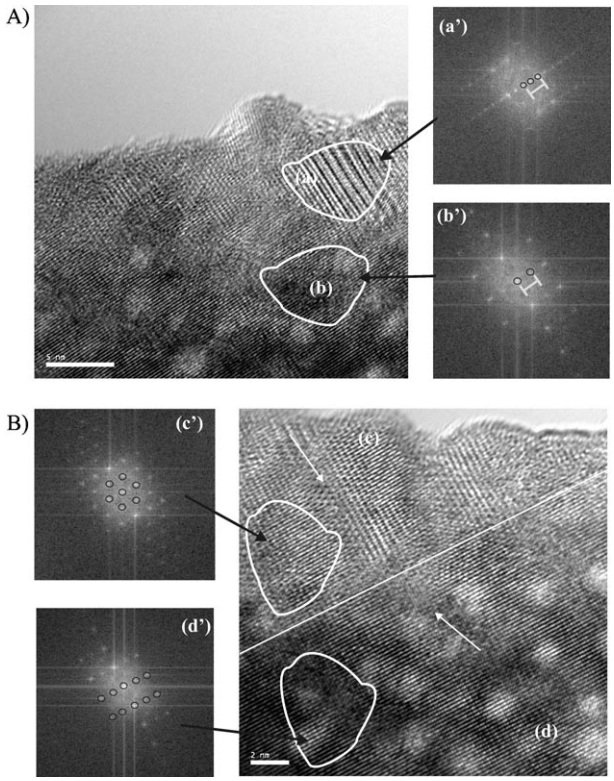

Figure 3. A) HRTEM image (left; scale bar: 5 nm) of a selected part of a $Na_{0.95}Pb_{20}SbTe_{22}$ sample, showing the coexistence of domains (a) and (b) with different features. The corresponding FFTs (a′) and (b′) (right) indicate that in one direction the periodicity of domain (a) is doubled compared to that of domain (b) (spacing indicated). B) HRTEM image (right; scale bar: 2 nm) of a selected part of a $Na_{0.95}Pb_{20}SbTe_{22}$ sample, consisting of two areas (c) and (d). The corresponding FFTs (c′) and (d′) (left) reveal that area (c) has a [111] orientation and area (d) a [011] orientation. The white arrows in the HRTEM image indicate crystal boundaries between domains of similar orientation. The white line across the HRTEM image, which divides the two areas, is drawn over one atomic row and traverses domains of type (c) and (d), without a shift in atomic row. See Supporting Information for measurement details.[28]

which surrounds domain (a). The nanocrystal domains of type (a) have compositions rich in Na and Sb. Figure 3B shows another area of nanoscale inhomogeneity elsewhere in the sample, in which two areas (c) and (d) have different orientations, [111] and [011], as revealed by the corresponding FFTs. The arrows indicate crystal boundaries between domains of similar orientation. Both domains are coherently grown; this feature is called endotaxy and is important in preserving facile charge transport through the sample, owing to reduced scattering.[2,22] This growth process creates interfaces between Na,Sb-rich, and Pb-rich regions. The Pb-rich regions are indicated by the slightly larger lattice spacing evident in the images (PbTe (NaCl type, $Fm\bar{3}m$) has a larger lattice spacing than $NaSbTe_2$).

The abundance of nano-interfaces is also apparent in the larger-area view shown in Figure 4, in which the degree of dispersity of the nanocrystals can be better assessed. The nanostructuring of $Na_{0.95}Pb_{20}SbTe_{22}$ is a key feature, whose impact on the properties of the material needs to be further

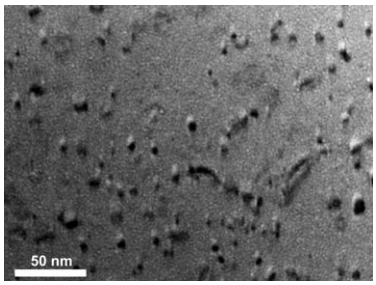

Figure 4. A low magnification TEM image of a $Na_{0.95}Pb_{20}SbTe_{22}$ sample, showing the evenly dispersed nanoscale features.

understood. To unequivocally support our view that this nanostructuring is largely responsible for the large drop observed in the lattice thermal conductivity in this system, we need the solid-solution version of these materials. The stabilization of real solid solutions of $Na_{1-x}Pb_mSb_yTe_{m+2}$, however, was not possible in our hands. Instead, we can compare the lattice thermal conductivity of $Na_{0.95}Pb_{20}SbTe_{22}$ with those of the well-known solid solutions of $PbTe_{1-x}Se_x$ and $Pb_{1-x}Sn_xTe$ for $x = 0.1$.[30,31] This x value represents the same degree of alloying of foreign atoms in the PbTe lattice for all three systems. Given the similar masses of the Sb, Se, and Sn atoms, we can expect that a true solid solution of composition $NaPb_{20}SbTe_{22}$ (that is, $(NaSbTe_2)(PbTe)_{20}$) for the same alloy fraction would produce a similar phonon scattering to those of $PbTe_{0.9}Se_{0.1}$ and $Pb_{0.9}Sn_{0.1}Te$. This hypothesis is, in fact, supported by the very similar lattice thermal conductivities of $\kappa_{latt} = 1.35$ and $1.44\ W m^{-1} K^{-1}$ for $PbTe_{0.9}Se_{0.1}$ and $Pb_{0.9}Sn_{0.1}Te$, respectively (Figure 5). Therefore, we expect a true solid solution of composition $NaPb_{20}SbTe_{22}$ to have

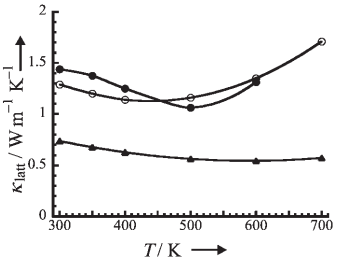

Figure 5. Comparison of the lattice thermal conductivity κ of $PbTe_{0.9}Se_{0.1}$ (○), $Pb_{0.9}Sn_{0.1}Te$ (●), and $Na_{0.95}Pb_{20}SbTe_{22}$ (▲). Data for $PbTe_{0.9}Se_{0.1}$ and $Pb_{0.9}Sn_{0.1}Te$ adapted from the literature.[30,31]

a comparable lattice thermal conductivity ($\kappa_{latt} \approx 1.4\ W m^{-1} K^{-1}$), but in contrast, we observe only half this value for $Na_{0.95}Pb_{20}SbTe_{22}$ (Figure 5). Thus, we can provide no other explanation for the reduced thermal conductivity of the $Na_{1-x}Pb_mSb_yTe_{m+2}$ materials, but to assign a significant role to the nanostructuring present in the samples.

Received: March 6, 2006
Published online: April 28, 2006

Keywords: lead · nanostructures · semiconductors · tellurides · thermoelectric materials

[1] *Thermoelectric Materials 2003–Research and Applications* (Eds.: G. S. Nolas, J. Yang, T. P. Hogan, D. C. Johnson), MRS Proceedings **2004**, *793*, references therein.
[2] G. Chen, M. S. Dresselhaus, G. Dresselhaus, J.-P. Fleurial, T. Caillat, *Int. Mater. Rev.* **2003**, *48*, 45 – 66.
[3] C. Wood, *Rep. Prog. Phys.* **1988**, *51*, 459 – 539.
[4] M. G. Kanatzidis, *Semicond. Semimetals* **2000**, *69*, 51 – 100.
[5] Z. M. Dashevsky, P. Dariel, S. Shusterman, *Semicond. Phys. Quantum Electron. Optoelectron.* **2000**, *3*, 181 – 184.
[6] M. Orihashi, Y. Noda, L.-D. Chen, T. Goto, T. Hirai, *J. Phys. Chem. Solids* **2000**, *61*, 919 – 923.
[7] R. Venkatasubramanian, T. Colpitts, E. Watko, M. Lamvik, N. El-Masry, *J. Cryst. Growth* **1997**, *170*, 817 – 821.
[8] T. C. Harman, D. L. Spears, M. J. Manfra, *J. Electron. Mater.* **1996**, *25*, 1121 – 1127.
[9] T. C. Harman, D. L. Spears, M. P. Walsh, *J. Electron. Mater.* **1999**, *28*, L1 – L4.
[10] T. C. Harman, P. J. Taylor, D. L. Spears, M. P. Walsh, *18th International Conference on Thermoelectrics* **1999**, 280 – 284.
[11] T. C. Harman, P. J. Taylor, M. P. Walsh, B. E. LaForge, *Science* **2002**, *297*, 2229 – 2232.
[12] C. Uher, *Semicond. Semimetals* **2000**, *69*, 139 – 253.
[13] B. C. Sales, D. Mandrus, R. K. Williams, *Science* **1996**, *272*, 1325 – 1328.
[14] I. Terasaki, Y. Ishii, D. Tanaka, K. Takahata, Y. Iguchi, *Jpn. J. Appl. Phys. Part 2* **2001**, *40*, L65 – L67.
[15] B. C. Sales, B. C. Chakoumakos, J. W. Sharp, D. Mandrus, *J. Solid State Chem.* **1999**, *146*, 528 – 532.
[16] G. S. Nolas, G. A. Slack, S. B. Schujman, *Semicond. Semimetals* **2001**, *69*, 255 – 300.
[17] S. Latturner, X. Bu, N. Blake, H. Metiu, G. Stucky, *J. Solid State Chem.* **2000**, *151*, 61 – 64.
[18] R. Venkatasubramanian, E. Siivola, T. Colpitts, B. O'Quinn, *Nature* **2001**, *413*, 597 – 602.
[19] H. Beyer, J. Nurnus, H. Bötner, A. Lambrecht, T. Roch, G. Bauer, *Appl. Phys. Lett.* **2002**, *80*, 1216 – 1218.
[20] J. C. Caylor, K. Coonley, J. Stuart, T. Colpitts, R. Venkatasubramanian, *Appl. Phys. Lett.* **2005**, *87*, 023105.
[21] K. F. Hsu, S. Loo, F. Guo, W. Chen, J. S. Dyck, C. Uher, T. Hogan, E. K. Polychroniadis, M. G. Kanatzidis, *Science* **2004**, *303*, 818 – 821.
[22] E. Quarez, K.-F. Hsu, R. Pcionek, N. Frangis, E. K. Polychroniadis, M. G. Kanatzidis, *J. Am. Chem. Soc.* **2005**, *127*, 9177 – 9190.
[23] E. Skrabeck, D. S. Trimmer, *CRC Handbook of Thermoelectrics* (Ed.: D. M. Rowe), CRC, Boca Raton, **1995**, p. 267.
[24] J. Androulakis, K. F. Hsu, R. Pcionek, H.-J. Kong, C. Uher, J. J. D'Angelo, A. Downey, T. Hogan, M. G. Kanatzidis, *Adv. Mater.* **2006**, in press.
[25] A. Khitun, K. L. Wang, G. Chen, *Nanotechnology* **2000**, *11*, 327 – 331.
[26] K. Hoang, K. Desai, S. D. Mahanti, *Phys. Rev. B* **2005**, *72*, 064102.
[27] D. Hicks, M. S. Dresselhaus, *Phys. Rev. B* **1993**, *47*, 12727 – 12731.
[28] Supporting Information available: synthesis procedures, measurement details, thermal-diffusivity, density, and specific-heat data, TEM sample-preparation procedure.
[29] A. F. Ioffe, *Semiconductor Thermoelements and Thermoelectric Cooling*, Infoserach, London, **1957**.
[30] E. D. Devyatkova, V. V. Tikhonov, *Sov. Phys.-Solid State* **1965**, *7*, 1427 – 1431.
[31] M. Orihashi, Y. Noda, L.-D. Chen, T. Hirai, *Mater. Trans. JIM* **2000**, *41*, 1196 – 1201.

